Expanded View Figures

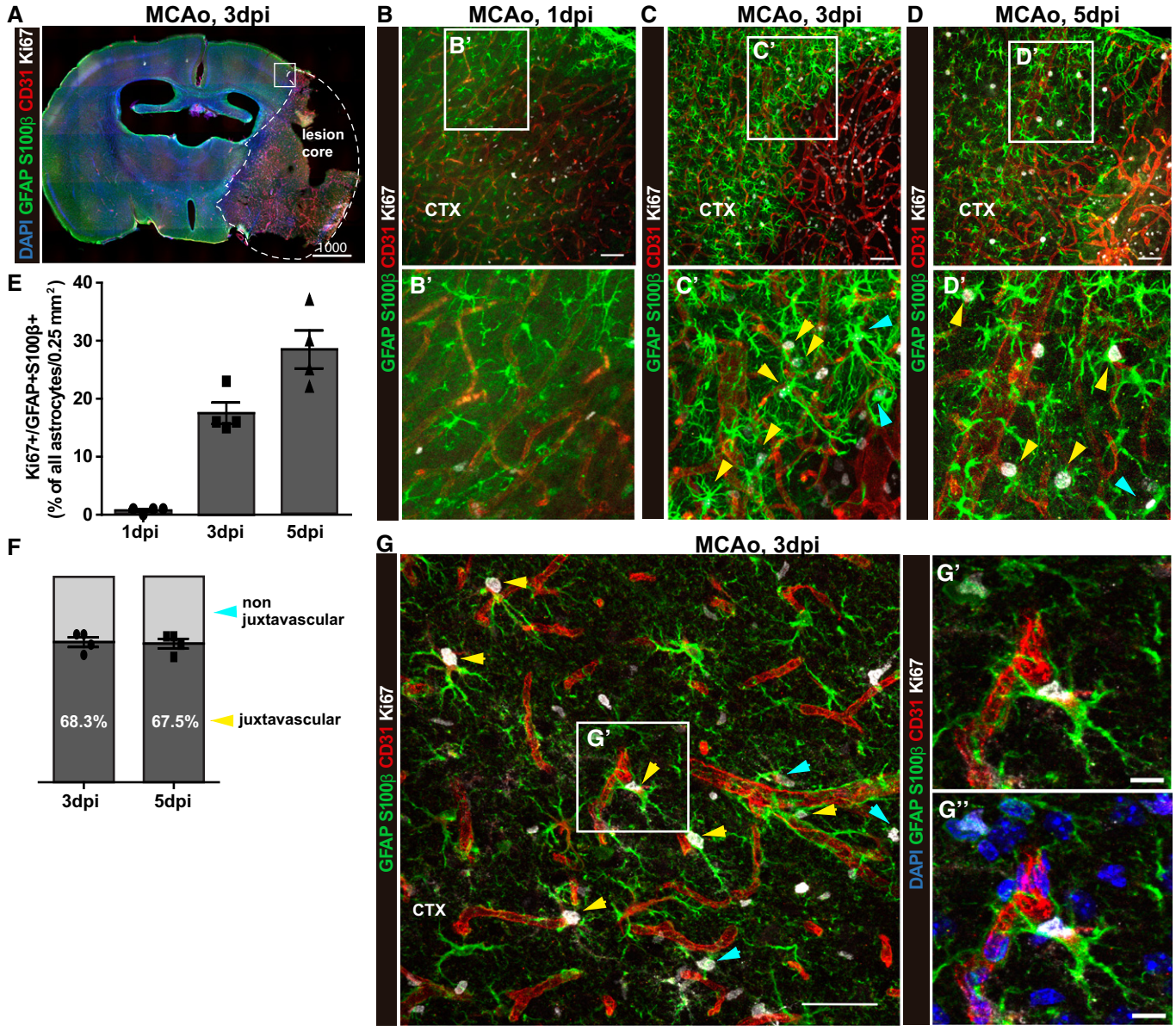

Figure EV1. Proliferation of astrocytes after MCAo is enriched at juxtavascular positions.

A Stitched tiles epifluorescence micrographs of a representative brain slice at 3 dpi post-MCAo. The lesion core is demarcated with a dashed line. A square shows the region of interest for quantifications.

B–D Confocal images from immunostaining for GFAP and S100β, Ki67, and blood vessels (CD31) from the penumbra of the ischemic lesion at 1, 3, and 5 dpi. Arrows point to proliferating astrocytes at juxtavascular positions (yellow) and not juxtavascular positions (cyan). The cell nuclei were counterstained with DAPI.

E, F Histograms depict the proportion of proliferating astrocytes among all (GFAP$^+$S100β$^+$) astrocytes in the lesioned GM (E) and the proportion of astrocytes proliferating at juxtavascular positions at 3 and 5 dpi (F). All data (individual data points, i.e., animals, are indicated as dots, triangles or squares) are represented as mean ± SEM per independent experiments (n = 4). Significance of differences between means was analyzed using one-way ANOVA followed by Tukey's multiple comparison test.

G High-power confocal micrographs of proliferating juxtavascular astrocytes (yellow arrows) with higher magnification in (G′ and G″) showing the maximum projection of 10 single optical planes of the Z-stack from the image shown in (G). Arrows point to proliferating astrocytes at juxtavascular positions (yellow) and not juxtavascular positions (cyan).

Data information: Scale bars: 1,000 μm (A), 100 μm (B–D), 25 μm (G, G′, G″).

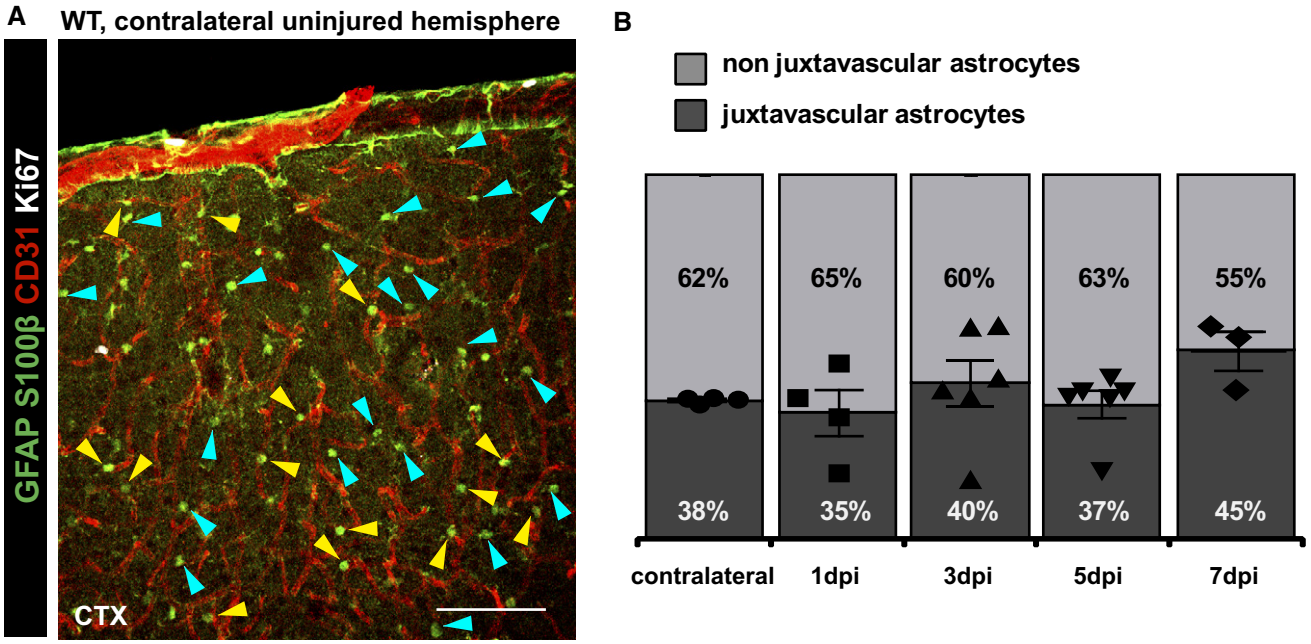

Figure EV2. Proportion of juxtavascular astrocytes in the GM.

A Confocal images of S100β and GFAP immunostaining labeling all astrocytes in the GM of the uninjured contralateral hemisphere co-stained for CD31 (vasculature) and Ki67 (proliferating cells). Arrowheads point to juxtavascular (yellow) and non juxtavascular (cyan) astrocytes in the uninjured GM parenchyma. Note that virtually no astrocytes proliferate in the uninjured site. Scale bar: 100 μm.

B Percentages of juxtavascular astrocytes among all GFAP/S100β immunolabeled astrocytes at different time points. All data (individual data points, i.e., animals, are indicated as separate symbols) are represented as mean ± SEM per independent experiments (n = 4 for the contralateral side and 1 dpi, n = 5 for 3 and 5 dpi, and n = 3 for 7 dpi). Significance of differences between means was analyzed using Kruskal–Wallis test, P = 0.0935.

Figure EV3. Microglia proliferation is increased after expression of SmoM2 in astrocytes by tamoxifen-mediated recombination in GLAST^{CreERT2}/SMOM2-YFP mice.

A Micrographs depict representative examples of immunostaining with Iba1, CD45, and CD31 in the injured GM of GLAST^{CreERT2}/SmoM2-YFP mice at 5 dpi.

B Higher magnification of the boxed areas (1 and 2 in A) showing CD45^{+}Iba1^{+} cells (cyan arrowheads) at the injury site and CD45^{+}Iba1^{-} cells accumulating in the vessels within the penumbra (yellow arrowheads in B1) or in the epimeningeal spaces (white arrowheads in B2). The dashed lines indicate the border between the epimeningeal space and cortical parenchyma. The cell nuclei were counterstained with DAPI.

C, D Representative confocal micrographs of Iba1 and Ki67 immunostaining in the lesioned cortex of WT controls (C) and GLAST^{CreERT2}/SmoM2-YFP mice (D). The dashed lines indicate the site of injury.

E The histogram displays total numbers of proliferating Ki67^{+} and Ki67^{+}Iba1^{+} microglia in both mouse lines at 5 dpi. Significance was tested with Mann–Whitney test (*P = 0.016, n = 5 for WT and n = 4 for SMOM2).

F Pie chart depicts the proportion of proliferating microglia among all proliferating cells at 5 dpi.

G, H Confocal pictures show more pronounced microgliosis toward the center of the lesion (dashed line) in a similar manner in both mice lines. Hypertrophic microglial cell bodies with thick processes are indicated by magenta arrowheads, and cyan arrowheads point to less reactive and more ramified microglial cells.

I, J Representative confocal images of NG2 and Ki67 immunostaining in the lesioned cortex GM of both lines.

K The histogram depicts the number of proliferating NG2^{+} cells with a significant increase in GLAST^{CreERT2}/SmoM2-YFP mice (Mann–Whitney test, *P = 0.035, n = 5 for WT and n = 3 for SMOM2).

Data information: Individual data points, that is, animals, are indicated as dots and squares, and the mean is indicated with SEM. Scale bars: 100 μm (A, C, D), 75 μm (G, H), 20 μm (B, I, J).

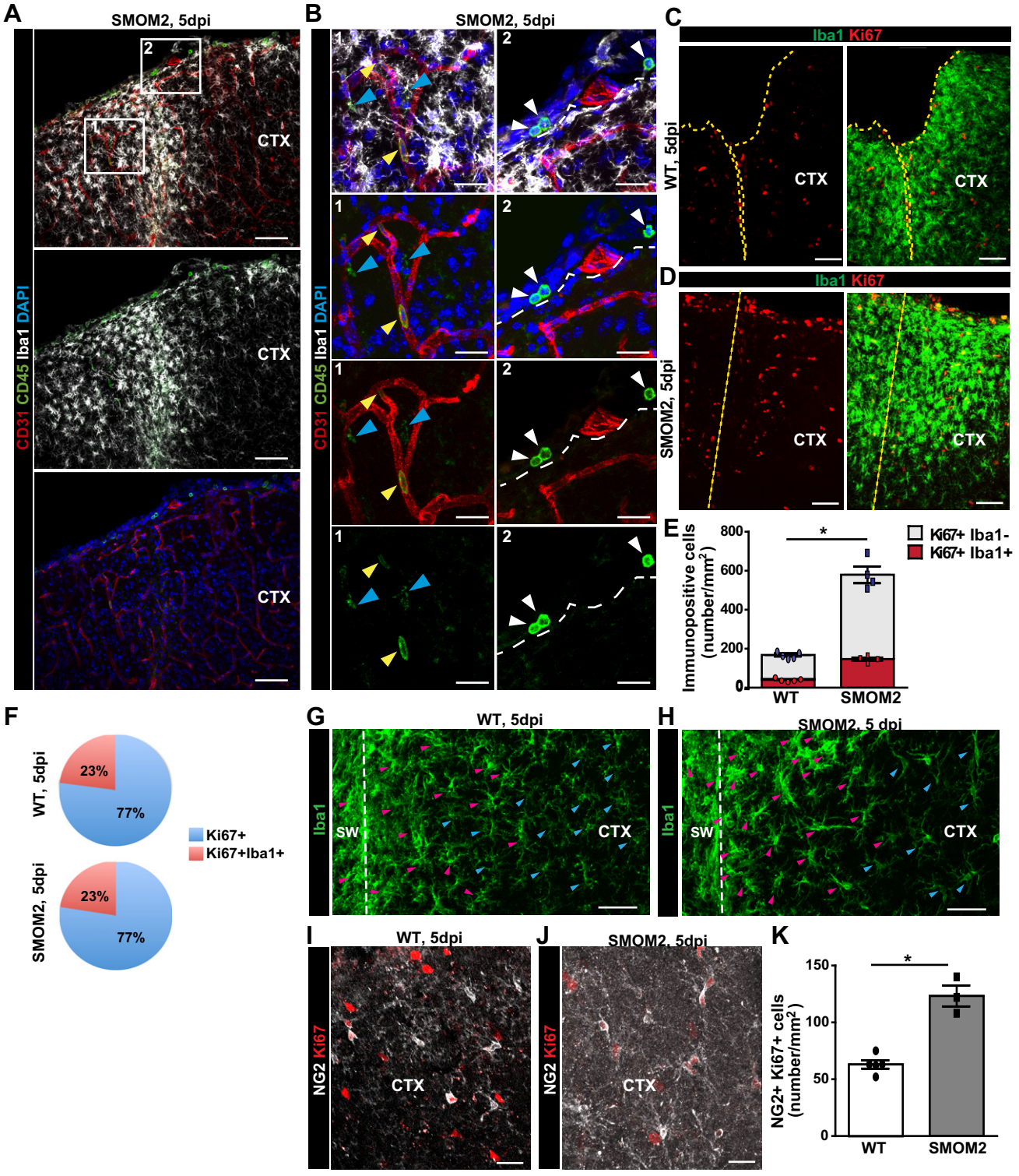
A
SMOM2, 5dpi
CD31 CD45 Iba1 DAPI
CTX
B
SMOM2, 5dpi
CD31 CD45 Iba1 DAPI
C
Iba1 Ki67
WT, 5dpi
CTX
D
Iba1 Ki67
SMOM2, 5dpi
CTX
E
Immunopositive cells (number/mm²)
Ki67+ Iba1-
Ki67+ Iba1+
WT
SMOM2
F
WT, 5dpi
SMOM2, 5dpi
23%
77%
Ki67+
Ki67+Iba1+
G
WT, 5dpi
Iba1
SW
CTX
H
SMOM2, 5 dpi
I
WT, 5dpi
NG2 Ki67
J
SMOM2, 5dpi
K
NG2+ Ki67+ cells (number/mm²)

Figure EV3.

Figure EV4. CCR2 deficiency impairs immune cell infiltration into the injured parenchyma.

A, B Confocal images of Iba1 and CD45 double-immunostaining in WT (A) and CCR2$^{-/-}$ (B) mice at 3 dpi. The cell nuclei were counterstained with DAPI.

C, D Overview of the lesioned cortex in heterozygous CCR2$^{RFP/+}$ (C) and homozygous CCR2$^{RFP/RFP}$ (D) mice.

E Confocal images of immune cell infiltrates at 5 dpi show co-localization of RFP expression and CD45. Pie graphs display the proportion of CD45 cells that were also RFP^{+} at 3 and 5 dpi.

F, G RFP expressing cells were detected in the parenchyma in heterozygous (F), but not in homozygous CCR2$^{RFP/RFP}$ mice where they remained inside blood vessels (G).

H, I Histograms depicting the number of proliferating glial cells at 3 dpi (H) (ns, $P = 0.2286$ for all Ki67^{+} cells, $n = 4$ for WT and $n = 3$ for CCR2$^{-/-}$; $P = 0.1143$ for Iba1^{+}Ki67^{+}, $n = 4$ WT, $n = 3$ CCR2$^{-/-}$; $P = 0.600$ for GFAP^{+}Ki67^{+}, $n = 3$) and the proportion of juxtavascular proliferating astrocytes among all proliferating astrocytes at the injury site of WT and CCR2$^{-/-}$ mice at 5 dpi (I). All data (individual data points, i.e., animals, are indicated as dots or squares) are represented as mean ± SEM per independent experiments ($n \geq 3$). Significance of differences between means was analyzed using Mann–Whitney test.

Data information: The dashed lines indicate the site of injury. Scale bars: 150 μm (C, D), 100 μm (A, B), 30 μm (F, G).

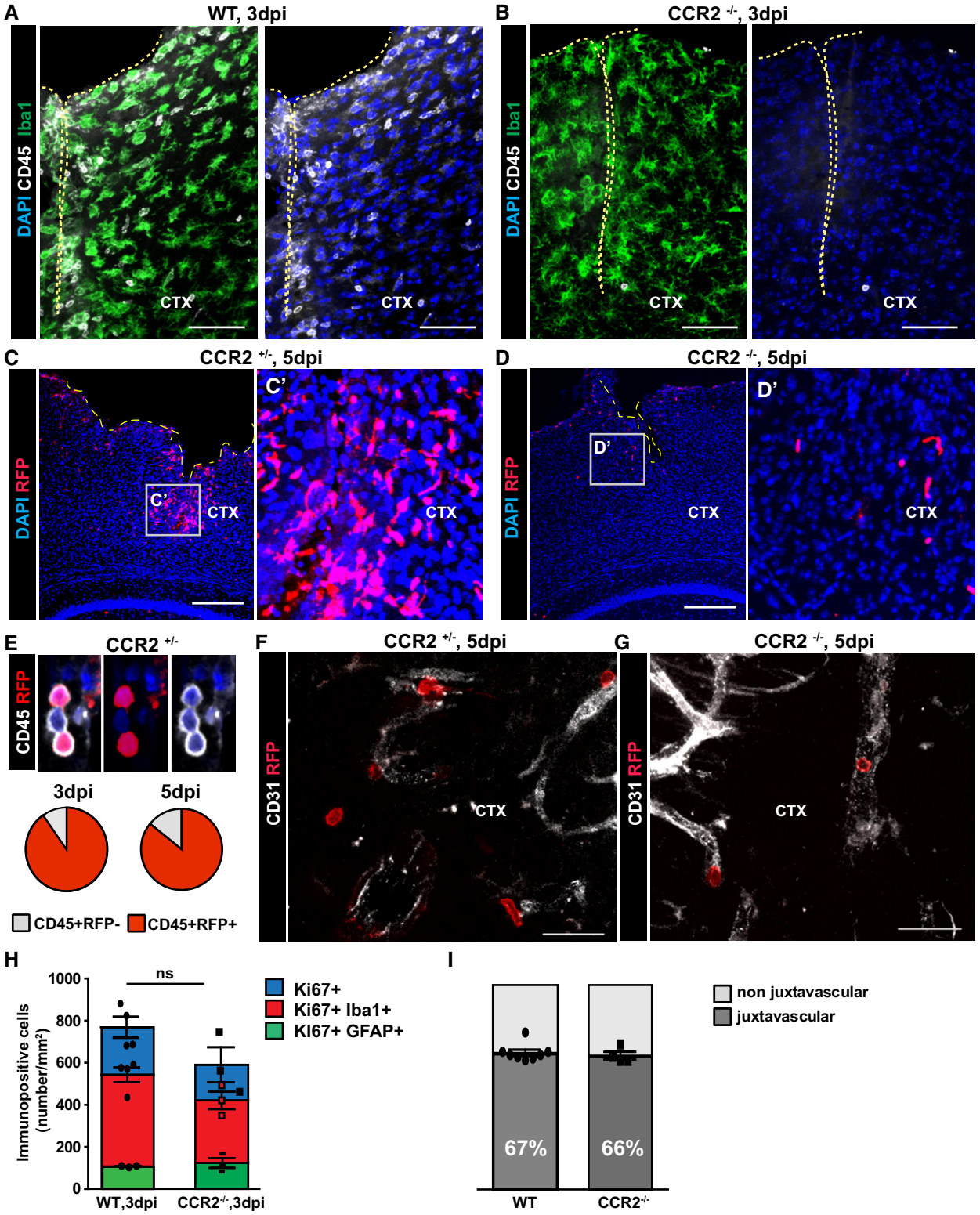
A
WT, 3dpi
DAPI CD45 Iba1
CTX
B
CCR2 -/-, 3dpi
C
CCR2 +/-, 5dpi
DAPI RFP
C'
D
CCR2 -/-, 5dpi
D'
E
CCR2 +/-
CD45 RFP
3dpi
5dpi
CD45+RFP-
CD45+RFP+
F
CCR2 +/-, 5dpi
CD31 RFP
G
CCR2 -/-, 5dpi
H
Immunopositive cells (number/mm²)
ns
Ki67+
Ki67+ Iba1+
KI67+ GFAP+
WT,3dpi
CCR2-/-,3dpi
I
non juxtavascular
juxtavascular
67%
66%
WT
CCR2-/-

Figure EV4.

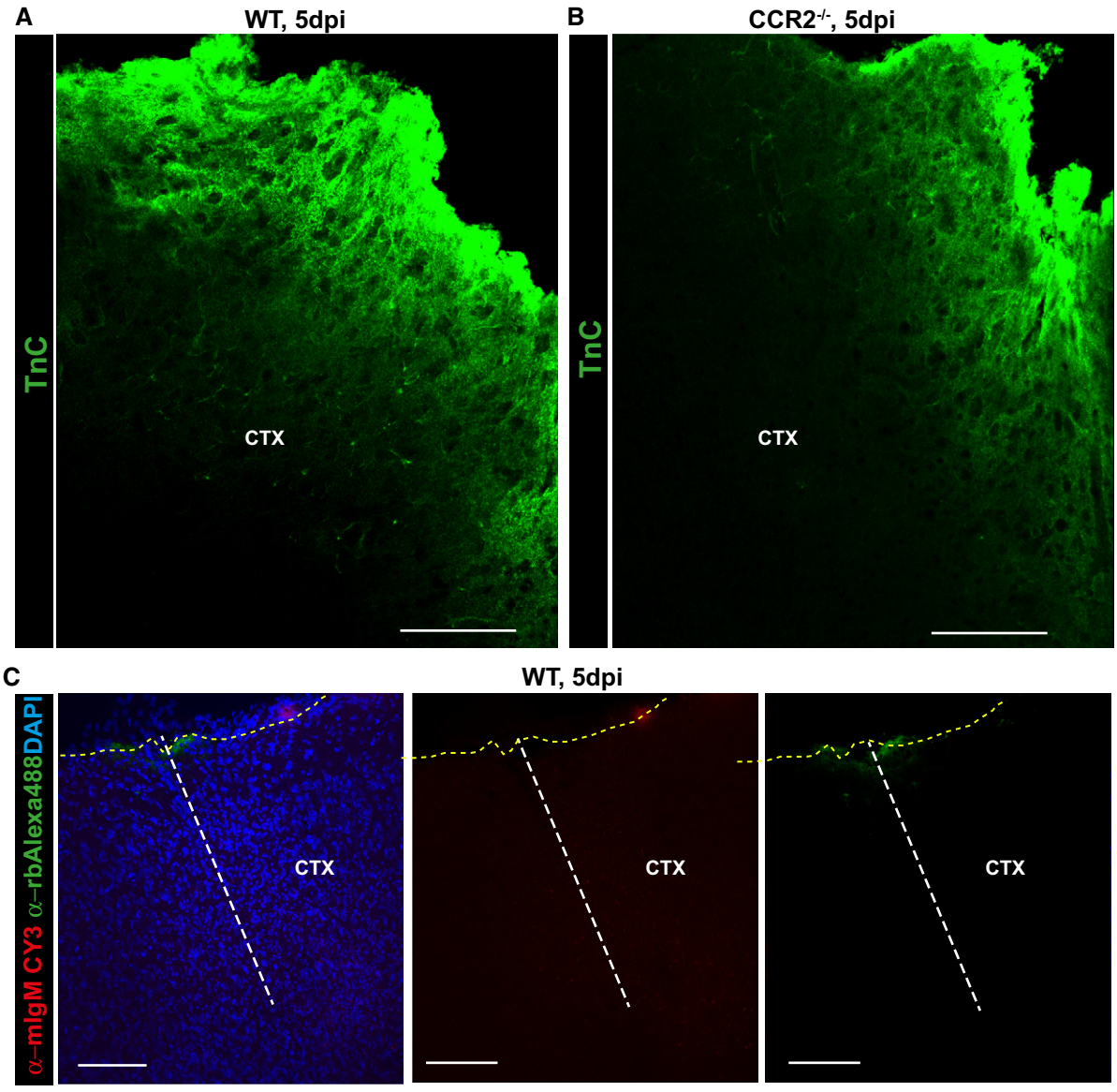

Figure EV5. Tenascin-C is reduced in the penumbra of CCR2$^{-/-}$ mice after stab wound injury.

A–C Confocal images displaying tenascin-C (Tn-C) immunostaining in the injured GM from WT (A) and CCR2$^{-/-}$ (B) mice at 5 dpi. Confocal images of control staining with only the secondary antibodies as indicated in the panel used for immunolabeling of ECM components showing absence of non-specific binding of these antibodies at injury site (C). The dashed lines indicate the site of injury (white) and the pial surface (yellow). The cell nuclei were counterstained with DAPI. Scale bars: 75 μm (A, B), 150 μm (C).